Crystal Structure of a Molybdopterin Synthase−Precursor Z Complex: Insight into Its Sulfur Transfer Mechanism and Its Role in Molybdenum Cofactor Deficiency[†,‡]

Juma N. Daniels,[§] Margot M. Wuebbens,[||] K. V. Rajagopalan,[||] and Hermann Schindelin*[,§,⊥]

Department of Biochemistry and Cell Biology, Stony Brook University, Stony Brook, New York 11794-5215, Department of Biochemistry, Duke University Medical Center, Durham, North Carolina 27710, and Rudolf Virchow Center for Experimental Biomedicine and Institute of Structural Biology, University of Würzburg, Versbacher Strasse 9, D-97078 Würzburg, Germany

Received August 26, 2007; Revised Manuscript Received October 23, 2007

ABSTRACT: In almost all biological life forms, molybdenum and tungsten are coordinated by molybdopterin (MPT), a tricyclic pyranopterin containing a *cis*-dithiolene group. Together, the metal and the pterin moiety form the redox reactive molybdenum cofactor (Moco). Mutations in patients with deficiencies in Moco biosynthesis usually occur in the enzymes catalyzing the first and second steps of biosynthesis, leading to the formation of precursor Z and MPT, respectively. The second step is catalyzed by the heterotetrameric MPT synthase protein consisting of two large (MoaE) and two small (MoaD) subunits with the MoaD subunits located at opposite ends of a central MoaE dimer. Previous studies have determined that the conversion of the sulfur- and metal-free precursor Z to MPT by MPT synthase involves the transfer of sulfur atoms from a C-terminal MoaD thiocarboxylate to the C-1′ and C-2′ positions of precursor Z. Here, we present the crystal structures of non-thiocarboxylated MPT synthase from *Staphylococcus aureus* in its apo form and in complex with precursor Z. A comparison of the two structures reveals conformational changes in a loop that participates in interactions with precursor Z. In the complex, precursor Z is bound by strictly conserved residues in a pocket at the MoaE dimer interface in close proximity of the C-terminal glycine of MoaD. Biochemical evidence indicates that the first dithiolene sulfur is added at the C-2′ position.

The transition metals molybdenum and tungsten are found in trace amounts in virtually all biological life forms and are required for a variety of redox transformations in prokaryotes, archaea, and eukaryotes. With the exception of nitrogenase, all Mo-dependent enzymes complex the metal via the molybdenum cofactor (Moco),[1] the biosynthetic pathway of which is well conserved in the three kingdoms of life (*1*, *2*). Moco is an essential component of proteins such as xanthine oxidase, sulfite oxidase, and nitrate reductase that are involved in the global carbon, sulfur, and nitrogen cycles (*2*−*7*). Therefore, the activity of these proteins depends on proper functioning of the enzymes involved in the biosynthesis of Moco. The metal-binding portion of Moco is usually termed molybdopterin (MPT) and can be chemically described as a reduced pyranopterin-ene-dithiolate with a terminal phosphate group as seen in Figure 1. In *Escherichia coli*, MPT biosynthesis starts with GTP which is converted to a sulfur-free tricyclic pyranopterin derivative, designated precursor Z, by the action of the MoaA and MoaC proteins (*8*−*10*). In the ensuing step, precursor Z is converted to MPT by MPT synthase. This heterotetrameric protein is composed of two subunits encoded by the *moaD* and *moaE* genes.

In the active form of MPT synthase, each MoaD molecule contains a thiocarboxylate at the C-terminal glycine that serves as the sulfur donor during synthesis of the MPT dithiolene group. Regeneration of the MoaD thiocarboxylate (MoaD-SH) is catalyzed by the MoeB protein in an ATP-dependent manner with the aid of a cysteine desulfurase and a rhodanese-like protein (*11*−*16*). The MoaD protein forms a stable, heterotetrameric complex with both MoaE (in MPT synthase) and MoeB. With the exception of the C-terminus, which is deeply buried in the partner protein, the MoaD structure is virtually identical in both complexes and is quite similar to the structure of ubiquitin (*11*, *14*). In the last conserved step of Moco biosynthesis, MPT is converted to Moco by complexation with molybdenum or tungsten, a step mediated by the MoeA and MogA proteins or their orthologs (*17*−*21*). In *E. coli*, an additional step of biosynthesis performed by the MobA protein results in the formation of the guanosine monophosphate-containing dinucleotide form of the cofactor (*22*, *23*). Upon completion of biosynthesis, mature Moco is inserted into the Moco-dependent enzymes, possibly with the aid of chaperones (*24*, *25*).

[†] This work has been supported by National Institutes of Health Grants GM00091 to K.V.R. and DK54835 to H.S.

[‡] The atomic coordinates and structure factors for *S. aureus* MPT synthase in its apo state (PDB entry 2Q5W) and in complex with precursor Z (PDB entry 2QIE) have been deposited in the Protein Data Bank.

* To whom correspondence should be addressed. Phone: +49 931 20148320. Fax: +49931 20148309. E-mail: hermann.schindelin@virchow.uni-wuerzburg.de.

[§] Stony Brook University.

[||] Duke University Medical Center.

[⊥] University of Würzburg.

[1] Abbreviations: Moco, molybdenum cofactor; MPT, molybdopterin; MoaD-SH, thiocarboxylated MoaD; IPTG, isopropyl thio-β-D-galactopyranoside; HPLC, high-performance liquid chromatography; rms, root-mean-square.

10.1021/bi701734g CCC: $40.75
Published on Web 12/20/2007

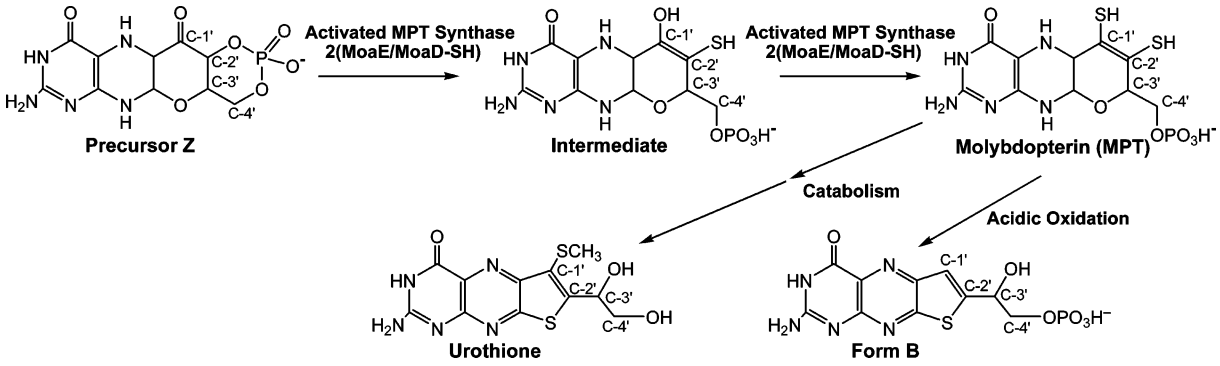

FIGURE 1: Structures of MPT and related molecules.

Mutations in the genes encoding the enzymes involved in human Moco biosynthesis lead to the rare and generally severe Moco deficiency disease (*26*, *27*). Affected patients display neurological symptoms such as attenuated growth of the brain, untreatable seizures, dislocated ocular lenses, and mental retardation, most often leading to death in early infancy. Moco deficiency has been categorized according to the Moco biosynthesis step in which the mutation occurs; group A patients have mutations in the genes involved in the first step of Moco biosynthesis (production of precursor Z), while group B patients carry mutations in genes encoding the proteins involved in either the conversion of precursor Z to MPT or metal incorporation (*27*). Mutations identified in group B patients include substitutions, deletions, and premature terminations in both *MOCS2A* and *MOCS2B*, the genes encoding the human equivalents of MoaD and MoaE, respectively (*27*−*29*).

The crystal structures of both active (thiocarboxylated) and inactive *E. coli* MPT synthase (PDB entries 3BII and 1FM0, respectively) as well as the MoaE homodimer have been previously determined (*11*, *14*). In the MPT synthase complex, the two MoaE molecules form a central dimer, with one MoaD located at each end, and the C-terminus of each MoaD molecule is deeply inserted into the adjacent (proximal) MoaE subunit. Structural and biochemical studies have localized the MPT synthase active site to a pocket lined with conserved residues at the interface between the distal and proximal MoaE subunits, which sits adjacent to the MoaD C-terminus that carries the thiocarboxylate when activated (*11*, *14*, *30*). The conversion of precursor Z to MPT involves the addition of sulfur atoms at the C-1′ and C-2′ side chain positions with the concomitant linearization of the cyclic phosphate bridging the C-2′ and C-4′ atoms. A monosulfurated, linear phosphate intermediate of this conversion has been identified during the catalytic cycle, verifying that the two sulfur atoms are added sequentially (*30*).

Although mass spectral analysis indicated the presence of a single sulfur atom on the intermediate side chain, the identity of the side chain carbon carrying the sulfur could not be determined (*30*). To clarify this and other aspects of the MPT synthase mechanism as well as to gain further insight into the etiology of MPT synthase mutations identified in cofactor deficient patients, the crystal structure of MPT synthase in complex with its substrate, precursor Z, was determined. Since the previously identified crystallization conditions for *E. coli* MPT synthase were not suitable for the growth of MPT synthase−precursor Z cocrystals (*11*, *14*), other organisms were screened to serve as the source of a MPT synthase protein that would crystallize under conditions more conducive for the visualization of a complex between MPT synthase and precursor Z. MPT synthase from *Staphylococcus aureus* proved amenable for this undertaking.

EXPERIMENTAL PROCEDURES

Expression and Purification of S. aureus MPT Synthase. For the His-tagged protein, the contiguous *S. aureus moaE* and *moaD* genes were PCR amplified from *S. aureus* genomic DNA (ATCC) to allow for cloning into the NdeI and BamHI sites of the pET-16b vector (Novagen), resulting in a hexa-His tag at the N-terminus of the MoaE protein. The resulting construct (pJD1000) was transformed into *E. coli* Rosetta (DE3) cells. For expression, 1 L cultures were induced at an OD_{600} of 0.5 with 0.5 mM isopropyl thio-β-D-galactopyranoside (IPTG) for 4 h at 37 °C. Cells were harvested at 4 °C by centrifugation at 16000*g* for 20 min and resuspended in 50 mM Tris-HCl, 300 mM NaCl, and 10 mM imidazole (pH 8.0). The suspension was passed twice through a French pressure cell and centrifuged at 75000*g* for 30 min at 4 °C. The clear lysate was applied to a Ni^{2+} agarose (Qiagen) column pre-equilibrated with lysis buffer. The column was then washed with the same buffer containing 20 mM imidazole, and the protein was eluted by increasing the imidazole concentration to 250 mM. Fractions containing MPT synthase were pooled and injected onto a Superdex 200 26/60 (GE Healthcare) size exclusion column pre-equilibrated with 50 mM Tris-HCl and 50 mM NaCl (pH 8.0). The eluted sample was concentrated to 10 mg/mL on the basis of a calculated molar extinction coefficient of 42 400 M^{-1} cm^{-1} using a 5 kDa Millipore Centricon Plus-20 concentrator. The typical yield of protein was ∼10 mg/L of cell culture.

To obtain nontagged *S. aureus* MPT synthase, PCR was used to incorporate NdeI and BamHI sites at the 5′ and 3′ ends, respectively, of the contiguous coding region for the MoaE and MoaD subunits from pJD1000. This DNA segment was then cloned into the pET-11b expression vector to generate plasmid pMWSaMPTS. All nucleotide sequences were verified by automated sequencing. This plasmid was transformed into *E. coli* BL21(DE3) cells for expression, and 1 L cultures in LB/carbenicillin medium were induced at an OD_{600} of 0.6 via addition of 0.1 mM IPTG. After growing for 5 h at 30 °C, the cells were harvested by centrifugation, resuspended in 10 mM Tris and 2 mM EDTA (pH 8.0), and stored at −20 °C. Protein purification was carried out as previously described for *E. coli* MPT synthase (*11*) using a Superdex 75 16/60 FPLC sizing column (GE Healthcare)

with a yield of approximately 25 mg/L of cell culture based on a calculated molar extinction coefficient of 43 973 M^{-1} cm^{-1}. For activity assays, the *S. aureus* MPT MoaE (pMWSaaE) and MoaD-SH (pMWSaaDSH) subunits were individually cloned, and these proteins as well as *E. coli* MoaE and MoaD-SH were purified and assayed as previously described for the *E. coli* MPT synthase subunits (*30*).

Preparation of MPT Synthase Loaded with Precursor Z. Precursor Z purification from the *moaD*$^-$ chlM(DE3) cell strain transformed with a plasmid expressing the MoaA protein followed a procedure similar to that described previously (*31*). Six 1 L LB/carbenicillin cultures were grown aerobically at 34 °C for 16 h. Cells were harvested by centrifugation, washed with H_2O, and resuspended in 2.8 mL of H_2O/g wet weight. The cells were divided into six aliquots, and each aliquot was treated sequentially as follows. The cells were acidified to pH 2 by the addition of 4 N HCl and centrifuged at 7600*g* for 10 min. The supernatant was neutralized with 2 N NaOH and rotoevaporated to a volume of approximately 0.9 mL which was injected onto an Alltech C18 HPLC column (14 mm × 250 mm) equilibrated with 5 mM ammonium acetate (pH 5.0). Precursor Z eluting between 3.5 and 5.0 mL was collected, pooled, and concentrated prior to injection onto an Alltech Partisil SAX HPLC column (14 mm × 250 mm) equilibrated with 10 mM sodium citrate (pH 3). The total amount of precursor Z purified from 6 L of culture was approximately 500 nmol in a volume of 2−3 mL. This was combined with 15 mL of 50 mM Tris-HCl and 50 mM NaCl (pH 8.0) prior to the addition of an equimolar amount of nontagged *S. aureus* MPT synthase. After incubation at 4 °C for 20 min, the mixture was concentrated to less than 1 mL. The volume was twice increased to 12.5 mL with additional buffer and then concentrated to a volume of less than 200 μL. The final sample concentration was 25−35 mg/mL MPT synthase.

Crystallization of S. aureus MPT Synthase. Tagged *S. aureus* MPT synthase was crystallized at a protein concentration of 10 mg/mL in a buffer containing 50 mM Tris-HCl and 50 mM NaCl (pH 8.0) against a precipitant consisting of 2.0 M sodium formate and 0.1 M sodium acetate (pH 5.3) at 22 °C. After 2 days, these conditions yielded spherulite bodies that transformed into well-defined crystals with approximate dimensions of 0.04 mm × 0.1 mm × 0.1 mm after 3 weeks. Since the high-salt/sodium formate crystallization conditions identified for the tagged MPT synthase were likely to prevent cocrystallization of the precursor Z complex, lower-salt crystallization conditions for the nontagged protein were screened. This protein crystallized under conditions consisting of 18% (w/v) PEG 8000, 0.1% polyvinylpyrrollidone K15, and 0.1 M Tris-HCl (pH 8.0) at 4 °C. Although this same condition did not initially yield diffraction-quality crystals for the precursor Z-loaded protein, the addition of microseeds of the untagged apo-protein resulted in cocrystals with dimensions of 0.22 mm × 0.14 mm × 0.14 mm after 3−4 days.

Data Collection, Structure Determination, and Refinement. For all samples, the crystals were soaked sequentially in increasingly higher concentrations of glycerol up to 30% and flash-cooled in liquid nitrogen. Diffraction data were collected at the National Synchrotron Light Source (Brookhaven National Laboratory, Upton, NY) at a wavelength of 1.1 Å on beamline X26C for apo *S. aureus* MPT synthase crystals and X25 for the precursor Z−MPT synthase cocrystals where the large *c*-axis necessitated a data collection protocol with a small ϕ increment. Diffraction data were indexed, integrated, and scaled using HKL-2000 (*32*). The structure of apo *S. aureus* MPT synthase was determined by molecular replacement with MOLREP (*33*, *34*) using the heterodimeric *E. coli* MPT synthase structure (*14*) as the search model. Rotational and translational searches were performed with data in the resolution range from 50 to 4 Å. The model was refined with REFMAC (*35*), initially by rigid body refinement followed by TLS and restrained refinement (*36*, *37*). Model building was carried out with O (*38*). Once a final model for the apoprotein was generated, MOLREP was used to find solutions for the complex structure. The precursor Z model was constructed utilizing the Monomer Library Sketcher from the CCP4 suite (*39*) starting with the structure of Moco. After an initial round of refinement of the MPT synthase structure without the substrate, precursor Z was positioned manually into the resulting electron density maps, while water molecules were added with ARP (*40*).

Generation of Form B from the Monosulfurated MPT Intermediate. An expression vector for the K123A variant of *S. aureus* MoaE (equivalent to *E. coli* K126A) was generated (pMWSaaEK123A), and the protein (*30*) as well as precursor Z (*31*) were purified as described previously. Two reaction mixtures containing either 80 nmol each of *S. aureus* MoaD-SH and K123A MoaE or *E. coli* MoaD-SH and K126A MoaE were combined and incubated for 10 min prior to the addition of 80 nmol of precursor Z and a quantity of 100 mM Tris (pH 7.2) sufficient to bring the total reaction volume to 2.5 mL. The reaction mixtures were left in the dark for 16 h at room temperature to facilitate production of the intermediate (*30*). At that point, both reaction mixtures along with a control reaction mixture containing human sulfite oxidase (a Moco-containing protein) were all acidified to pH 2.5 with 4 N HCl and placed in a boiling water bath for 30 min to generate Form B (*41*). After cooling and centrifugation to remove precipitated protein, each supernatant was applied to a separate PD-10 desalting column (GE Healthcare) equilibrated with 10 mM acetic acid. The columns were washed with 6.5 mL of the same solution prior to elution of Form B with an additional 4 mL. The pH of the reaction mixtures was increased to 8−9 with 2 N NaOH, followed by the addition of 10 μL of a calf intestine alkaline phosphatase (Roche) solution and 25 μL of 1 M $MgCl_2$. The three samples were left in the dark at room temperature for 16 h. Subsequently, each sample was concentrated to dryness, resuspended with 1.0 mL of H_2O, acidified to pH 5−6, and analyzed by injection onto an Alltech C18 HPLC column (250 mm × 4.6 mm) equilibrated with 50 mM ammonium acetate and 20% methanol with a flow rate of 1 mL/min (*41*, *42*).

RESULTS AND DISCUSSION

Cloning, Purification, and Analysis of S. aureus MPT Synthase. All previously identified crystallization conditions for the various forms of *E. coli* MPT synthase employ either high-salt conditions or extended crystallization times of weeks to months (*11*, *14*). Since high-salt conditions would be incompatible with the formation of MPT synthase−precursor Z cocrystals, and precursor Z oxidizes within days

in solution, initial efforts were directed at discovering alternative conditions for crystallization of *E. coli* MPT synthase. When these efforts proved futile, MPT synthase proteins from other organisms were cloned, expressed, and screened for crystallization suitability. The MPT synthase protein from *S. aureus* was found to crystallize under more appropriate conditions, and this protein was chosen for further cocrystallization experiments. Expression vectors for His-tagged and native *S. aureus* MPT synthase as well as the individual *S. aureus* MoaE and MoaD-SH subunits were created.

The primary sequence identity of *E. coli* and *S. aureus* MPT synthase is 35.5 and 25.9% for the MoaE and MoaD subunits, respectively, and the strictly conserved residues identified in multiple-sequence alignments of *E. coli* MPT synthase are all present in the *S. aureus* protein, including those presumed to be involved in substrate binding and catalysis (*11*, *14*). *S. aureus* MoaE, MoaD-SH, and native MPT synthase were all purified under the same conditions as the *E. coli* proteins, with similar protein yields (*11*, *30*). To assay for *S. aureus* MPT synthase activity (production of MPT from precursor Z), the individual *S. aureus* and *E. coli* activated MPT synthase subunits were combined with precursor Z (*30*). When compared to that of the *E. coli* protein, the rate of MPT production by activated *S. aureus* MPT synthase was approximately 5.5 times slower with $t_{1/2}$ values of 1.65 and 0.3 min, respectively, although the final extent of MPT production was the same for both synthases (data not shown).

Structure of Apo S. aureus MPT Synthase. His-tagged, apo *S. aureus* MPT synthase crystals belong to the monoclinic space group *C*2 with the following unit cell dimensions: $a = 133.9$ Å, $b = 45.8$ Å, $c = 41.8$ Å, and $\beta = 93.4°$ with one MoaD−MoaE heterodimer in the asymmetric unit. Although the crystals diffracted X-rays well beyond 2.0 Å resolution, the structure was refined at this resolution to an R_{factor} of 0.149 and an R_{free} of 0.193 (Table 1). The resulting model has good stereochemistry with 97.6% of all non-Pro and non-Gly residues in the most favored regions of the Ramachandran diagram, 2.4% in generously allowed regions, and no residues in disallowed regions as defined by MOLPROBITY (*43*). As seen in Figure 2A, both subunits of MPT synthase exhibit a mixed $\alpha+\beta$ architecture. The MoaD subunit adopts a ubiquitin-like fold which is composed of a central β-sheet consisting of five strands and three α-helices, while the MoaE subunit exhibits an α/β hammerhead fold and contains eight β-strands forming two β-sheets surrounded by a total of four α-helices.

Despite the relatively low level of sequence identity between the two proteins, the overall structure of *S. aureus* MPT synthase is quite similar to that of *E. coli* MPT synthase. This is reflected in root-mean-square (rms) deviations between C-α atoms of 1.45 and 1.2 Å, if the MoaE and MoaD subunits, respectively, are superimposed. In contrast, a superposition of the entire MoaE−MoaD heterotetramer results in a somewhat larger rms deviation of 1.7 Å due to the fact that the *E. coli* and *S. aureus* MoaD subunits in the MPT synthase complexes differ by a rotation of ∼17° around the C-terminal tail. Further examination of the highly conserved residues forming the MoaD−MoaE interface in the two MPT synthase complexes (*S. aureus* MoaD Phe6, Ala7, Phe55, and Ile71 corresponding to *E. coli* Phe7, Ala8, Leu59, and Phe75, respectively, and *S. aureus* MoaE Tyr52, Met55, Trp122, and Trp133 corresponding to *E. coli* Tyr55, Met58, Trp125, and Trp136, respectively) reveals that these residues interact in a similar fashion despite the MoaD rotation. Interestingly, the type-conserved exchange of *E. coli* MoaD Phe75 with Ile71 of *S. aureus* MoaD is complemented by a reverse exchange of *E. coli* MoaD Leu59 with Phe55 of *S. aureus* MoaD at a nearby position, thus preserving the structural framework of the interface as seen in Figure 2B.

A noteworthy difference between the two structures is that residues 36−44 of the *S. aureus* MoaE subunit are ordered while the corresponding residues (39−47) in *E. coli* MoaE were disordered in all crystal structures (*11*, *14*). With the presence of this loop, a distinct cavity adjacent to the postulated active site is formed which is visible when a surface representation of the structure is calculated as seen in Figure 2C. On the other hand, the C-terminus of *S. aureus* MoaE (residues 135−149) corresponding to the last helix of *E. coli* MoaE is disordered. When the C-terminal region of *S. aureus* MoaE is modeled on the basis of the *E. coli* structure, Gln137 would partially occlude the binding pocket

Table 1: Crystallographic Data[a]

	apoenzyme	precursor Z complex
Data Collection		
space group	*C*2	$P222_1$
unit cell dimensions	$a = 133.9$ Å	$a = 56.6$ Å
	$b = 45.8$ Å	$b = 58.1$ Å
	$c = 41.8$ Å	$c = 331.8$ Å
	$\alpha = 90°$	$\alpha = 90°$
	$\beta = 93.4°$	$\beta = 90°$
	$\gamma = 90°$	$\gamma = 90°$
resolution limits	50−2.0	50−2.5
completeness	0.948 (0.714)	0.969 (0.830)
R_{sym}[b]	0.033 (0.065)	0.071 (0.632)
$\langle I/\sigma I\rangle$[c]	42.0 (15.4)	22.2 (2.4)
redundancy	3.3 (2.1)	5.3 (3.6)
no. of reflections	54634	200513
no. of unique reflections	16442	38004
Refinement		
no. of reflections used	15541	36033
resolution limits	30−2.0	30−2.5
no. of protein/solvent/ substrate atoms	1751/152	7004/78/92
R_{factor}[d]	0.149	0.206
R_{free}[e]	0.193	0.255
rms deviation from ideal values		
bond distances (Å)	0.017	0.009
bond angles (deg)	1.55	1.21
chiral centers (Å^3)	0.10	0.071
average *B*-factor (Å^2) of protein/solvent atoms	28.0/30.9/−	61.7/66.6/87.0
average *B*-factor (Å^2)		
of cofactors and surrounding	−	73/79/94/109
atoms within a 5 Å radius	−	64/65/70/71
Ramachandran statistics[f]	97.6/0.0	97.8/0.0

[a] Numbers in parentheses apply to the respective highest-resolution shell. [b] $R_{sym} = \sum_{hkl}\sum_i|I_i - \langle I\rangle|/\sum_{hkl}\sum_i I_i$, where I_i is the ith measurement and $\langle I\rangle$ is the weighted mean of all measurements of I. [c] $\langle I/\sigma I\rangle$ indicates the average of the intensity divided by its standard deviation. [d] $R_{factor} = \sum||F_o| - |F_c||\sum|F_o|$, where F_o and F_c are the observed and calculated structure factor amplitudes, respectively. [e] R_{free} is the same as R_{factor} for 5% of the data randomly omitted from refinement. [f] Ramachandran statistics indicate the fraction of residues in the most favored and disallowed regions of the Ramachandran diagram as defined by MOLPROBITY (*43*).

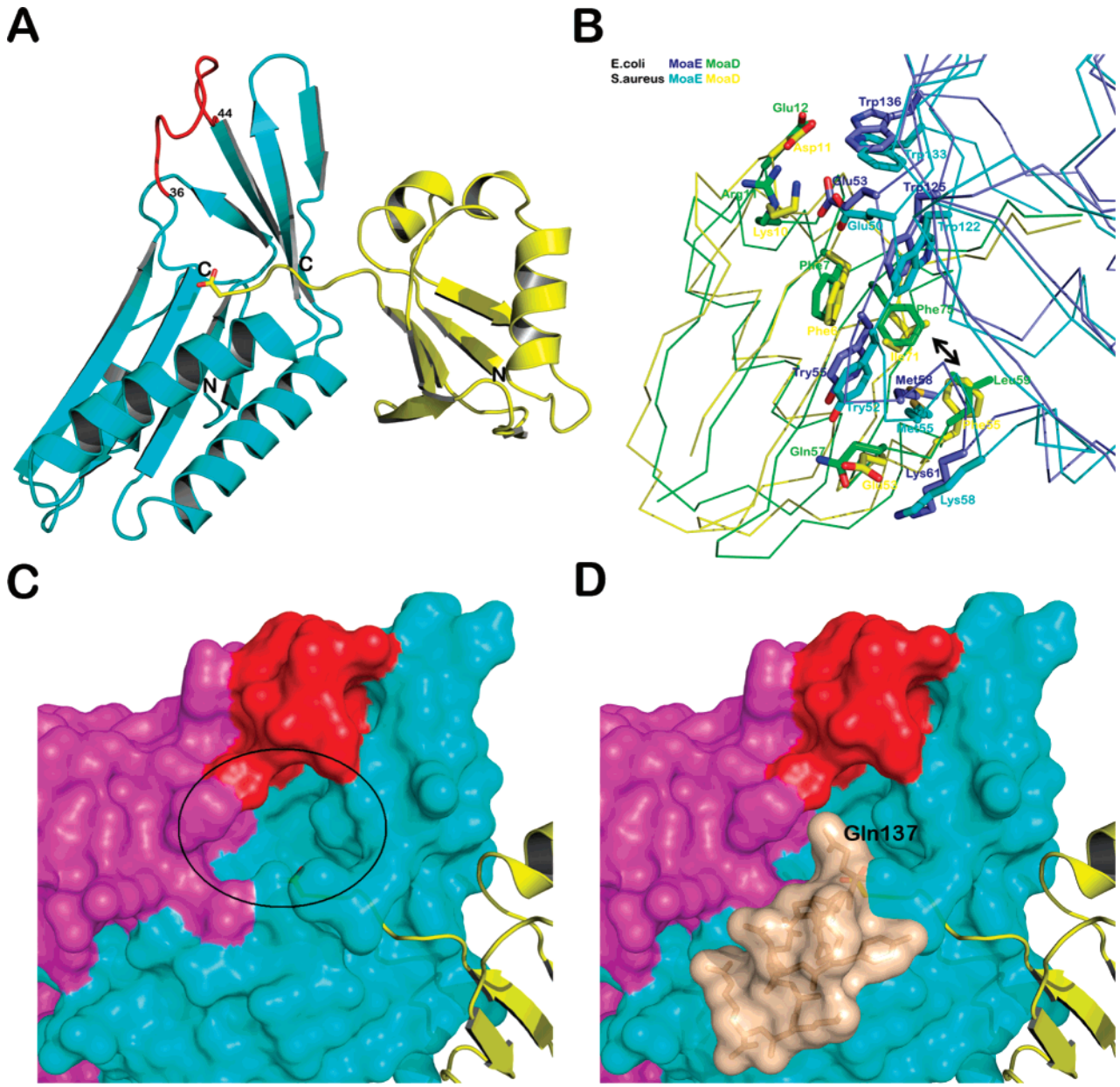

FIGURE 2: Structural features of *S. aureus* MPT synthase. (A) Ribbon diagram of *S. aureus* apo-MPT synthase with MoaE (cyan) and MoaD (yellow), and the newly ordered loop, residues 36−44, colored red. (B) Superposition (based on the MoaE and MoaD subunits) and conservation of the MoaE−MoaD interface in *E. coli* and *S. aureus* MPT synthase. The α-carbons are colored as follows: cyan for *S. aureus* MoaE, yellow for *S. aureus* MoaD, blue for *E. coli* MoaE, and green for *E. coli* MoaD. The interface side chain residues are depicted in all-bonds representation. The conserved exchange between residues of *E. coli* and *S. aureus* MoaD is highlighted with an arrow. (C) Surface representation of the substrate-free MPT synthase heterotetramer with MoaE subunits (cyan and magenta) and residues 36−44 (red). MoaD is shown as a ribbon diagram (yellow) with its C-terminal carboxylate in all-bonds representation depicted inside the MoaE cavity (black ellipse). (D) Model of the C-terminal region of *S. aureus* MoaE (tan) modeled on the basis of the *E. coli* MPT synthase structure.

(Figure 2D). Gln137 is replaced by Arg140 in *E. coli* MoaE, and this longer residue would almost completely block the active site, suggesting that the conformation observed for the C-terminal residues of *E. coli* MoaE is not compatible with substrate binding.

Last, the *S. aureus* MoaE β-strands formed by residues 45−52, 81−90, and 121−136 are all in the vicinity of the ordered loop of residues 36−44 and exhibit shifts of up to 6 Å for main chain atoms when compared to the *E. coli* structure. It is unclear whether these shifts are due to residues 36−44 becoming ordered or if they reflect true structural differences between *S. aureus* and *E. coli* MPT synthase. Although there are hydrophobic interactions between the side chains of residues located in these strands and their symmetry mates (with Trp38, Val42, and Lys43 contacting symmetry mates Ile75, Tyr24, and Phe19), crystal packing effects can be excluded as the source of the structural changes in this region since a similar conformation is also observed in the complex of *S. aureus* MPT synthase and precursor Z, described below, where the packing is quite different.

Structure of S. aureus MPT Synthase in Complex with Precursor Z. The cocrystals diffracted X-rays up to 2.5 Å resolution and belong to the orthorhombic space group $P222_1$ with the following unit cell dimensions: $a = 56.6$ Å, $b = 58.1$ Å, and $c = 331.8$ Å containing two MoaD−MoaE heterotetramers in the asymmetric unit. The structure of the

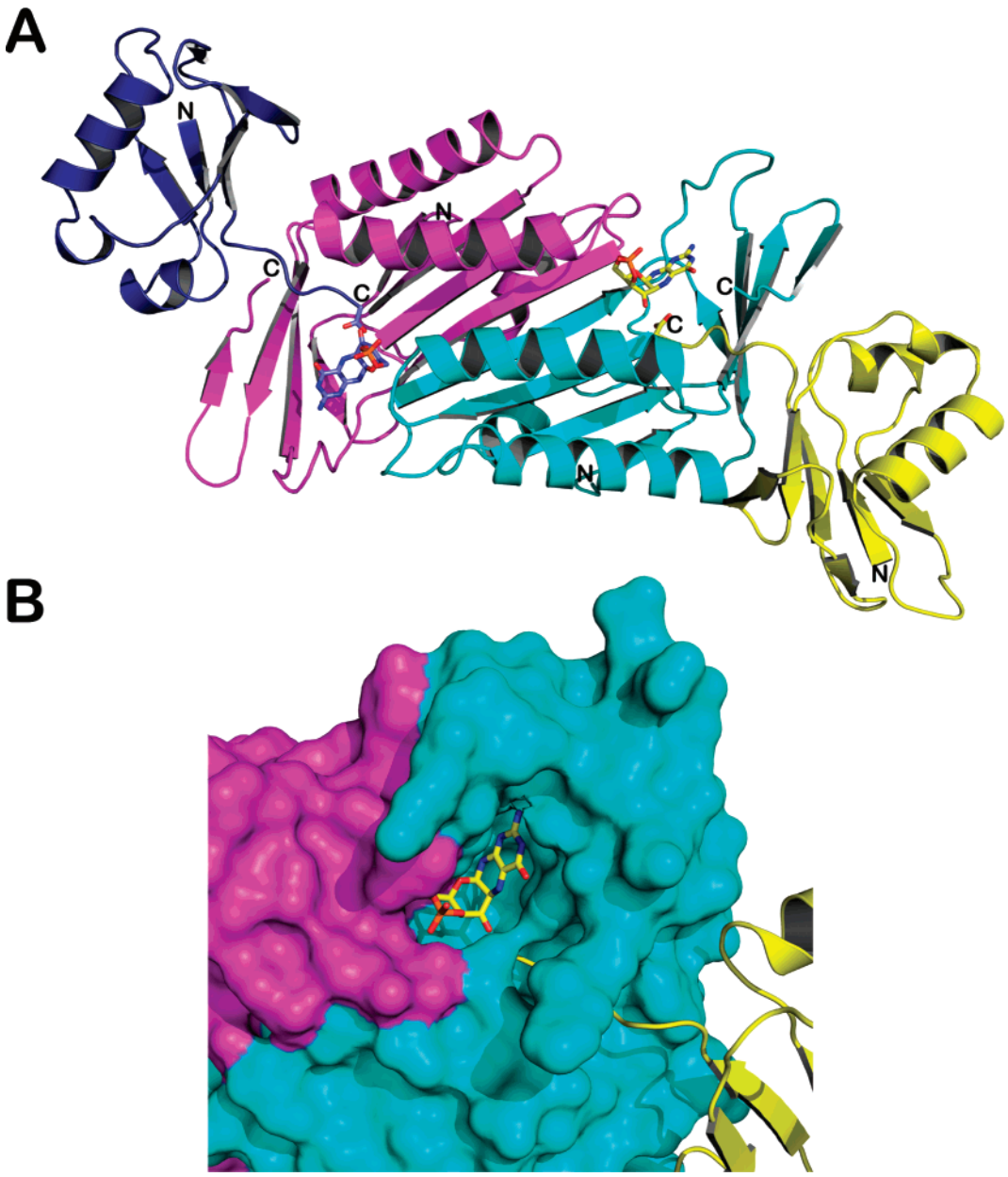

FIGURE 3: Structure of *S. aureus* MPT synthase in complex with precursor Z. (A) Ribbon diagram of the *S. aureus* MPT synthase heterotetramer with MoaE (magenta and cyan) and MoaD (dark blue and yellow). The C-terminal carboxylates and precursor Z are shown in all-bonds representation. The precursor Z carbon atoms are colored according to the adjacent MoaD subunit (dark blue and yellow). (B) Surface representation of the proximal MoaE (cyan) and distal MoaE (magenta) with precursor Z in all-bonds representation (yellow) and the adjacent MoaD subunit (yellow).

complex was refined to an R_{factor} of 0.206 and an R_{free} of 0.255, resulting in a model with good stereochemistry with 97.8% of all non-Pro and non-Gly residues in the most favored regions of the Ramachandran diagram (*43*), 2.2% in generously allowed regions, and no residues in disallowed regions (Table 1). Manual positioning of precursor Z into the unbiased electron density maps after refinement of only the protein atoms resulted in excellent fits for the substrate in three of the four heterodimers (A−B, H−G, and K−J) present in the asymmetric unit. As seen in Figure 3, precursor Z is bound in the postulated substrate-binding site, in the vicinity of the MoaD C-terminus and the MoaE dimer interface (*11*, *14*, *30*).

When the four MoaD−MoaE heterodimers in each asymmetric unit of the complex structure are compared to each other, there are small structural differences as reflected by an average pairwise rms deviation between C-α atoms of ~0.5 Å. The most pronounced structural differences between the heterodimers are seen in the loop encompassing residues 39−45. Interestingly, there is a correlation between the average *B*-factor of the precursor Z bound in the structure and the conformation of this loop. Heterodimers (A−B, H−G, and K−J) in which the bound precursor Z has an average *B*-factor of less than 80 Å^2 (indicating a high occupancy of precursor Z) adopt nearly identical loop conformations, whereas the heterodimer (E−D) in which the bound substrate has an average *B*-factor of greater than 100 Å^2 (indicating a lower occupancy of precursor Z) displays a conformational change resulting in a shift of the loop by approximately 5 Å. In this heterodimer, the loop adopts a conformation similar to the apo structure. Consequently, the overall rms deviation following superposition of C-α atoms

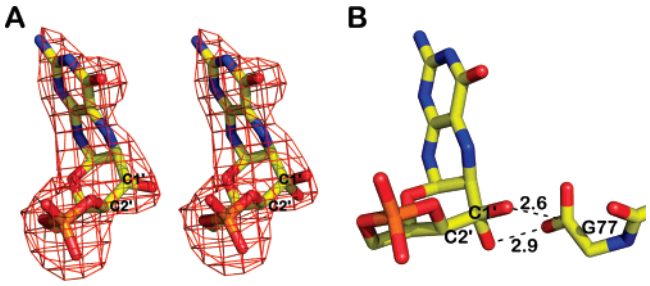

FIGURE 4: Precursor Z identification. (A) Omit difference density map contoured at 3.0σ (calculated after refinement in REFMAC in the absence of precursor Z), superimposed with the keto (left) and geminal diol (right) forms of precursor Z (C atoms colored yellow, N atoms blue, O atoms red, and P atom orange). The C-1′ and C-2′ positions are labeled. (B) The short distances between the geminal diol and C-terminal glycine are highlighted.

between this heterodimer and the apo structure is smaller (0.6 Å) compared to the average rms deviation between the apo structure and the heterodimers which display lower *B*-factors for the substrate (average rms deviation of ∼0.7 Å). These observations suggest that the loop conformation is coupled to the presence or absence of substrate in the active site.

Chemical Structure of Precursor Z. The chemical structure of precursor Z was originally determined by Wuebbens and Rajagopalan and is shown in Figure 1 (*31*, *44*). However, a subsequent paper by Santamaria et al. (*45*) describing precursor Z analysis by ^{1}H NMR reported a slightly different structure with a geminal diol at the C-1′ position instead of a keto group. For the precursor Z structure in the cocrystals, both possible structures were considered. While both fit an omit difference density map equally well (Figure 4A), the distances between the C-terminal glycine of MoaD and the geminal diol are rather short (Figure 4B), resulting in greater steric hindrance than in the carbonyl model. Therefore, the original precursor Z structure containing the C-1′ keto group was used as the model for the cocrystal structure. Since geminal diols readily dehydrate to form a carbonyl, both models are chemically similar, and it is possible that precursor Z can exist in either or both forms depending on the solvent and protein environment.

MPT Synthase Active Site. The structure of MPT synthase in complex with precursor Z defines the active site of the enzyme in significantly more detail than in the previously published *E. coli* MPT synthase structures where the assignment was based on the presence of highly conserved, surface-exposed residues (*11*, *14*). These conserved residues included Phe34, Arg39, His103, Arg104, Met115, Lys119, and Lys126 of *E. coli* MoaE, which correspond to *S. aureus* residues Phe31, Arg36, His100, Arg101, Ile112, Lys116, and Lys123, respectively. A His-Arg pair in both structures (His103-Arg104 in *E. coli* MoaE and His100-Arg101 in *S. aureus* MoaE) is located in the distal MoaE subunit and has been shown to coordinate a sulfate ion in one of the crystal forms of *E. coli* MPT synthase (*14*).

As described for the *S. aureus* apo structure, the precursor Z binding pocket is located at the conjunction of the MoaE dimer interface and the MoaD C-terminus in each heterodimer of the MPT synthase heterotetramer. The MoaD C-terminus gains access to the active site by threading through the MoaE subunit from the opposite side, and the active site pocket is a predominately positively charged molecular surface that embraces the negatively charged C-terminus of MoaD. In the complex structure, the substrate fits nicely into the MoaE cavity lined with highly conserved residues (Figure 5A). The strictly conserved Phe31 residue is part of a small hydrophobic patch adjacent to the substrate which also includes the type-conserved residues Val92 and Ile112 (Figure 5B). Arg36 stacks via a cation−π interaction with the precursor Z pterin ring system. The positively charged residues His100 and Arg101 coordinate the cyclic phosphate of precursor Z, a role postulated previously from the structure of *E. coli* MPT synthase in complex with sulfate (*14*). Finally, the amino groups of Lys116 and Lys123 form hydrogen bonds with both the MoaD C-terminal carboxylate and the C-1′ oxygen of precursor Z with distances ranging from 2.5 to 3.1 Å. As mentioned before, conformational changes between the apo and complex structures occur in the loop formed by residues Thr39−Glu45. Thr39 and Thr44 in this loop interact with Arg36 and the pterin NH_2 group of precursor Z. Comparison of the apo *S. aureus* MPT synthase structure and the substrate complex indicates few conformational changes in the active site except for the side chain of Arg36 which points away from the active site in the apo structure.

Implications for the Catalytic Mechanism of MPT Synthase. As mentioned previously, the conversion of precursor Z to MPT requires the addition of sulfur atoms at adjacent side chain carbons and the concomitant linearization of the precursor Z cyclic phosphate. Previous work with *E. coli* MPT synthase variants identified a pair of MoaE lysine residues at the active site proposed to be involved directly in the two sulfur transfer steps. *E. coli* Lys119 (*S. aureus* Lys116) has been implicated in the first sulfur transfer since the K119A variant is completely inactive. Lys126 (*S. aureus* Lys123) has been implicated in the second transfer since *E. coli* MPT synthase reaction mixtures containing the K126A MoaE variant accumulate large quantities of a reaction intermediate that is only present in small amounts in wild-type reaction mixtures (*30*). This intermediate is monosulfurated and tightly bound to the MPT synthase complex, indicating that each precursor Z molecule binds to a single active site where it remains bound until it is completely converted to MPT (*30*).

Although initial biochemical results indicated that the intermediate contained a linear phosphate, it was not possible to determine whether its single sulfur atom was located at C-1′ or C-2′. At first glance, the proximity between the MoaD C-terminal glycine and the precursor Z C-1′ atom in the cocrystal structure suggests that the first sulfur atom transferred from a MoaD thiocarboxylate would likely be incorporated at the C-1′ precursor Z position. However, since these crystals were formed from inactive MPT synthase that does not contain the thiocarboxylate group at the MoaD C-terminus, this structure represents a noncatalytic enzyme−substrate complex. In this inactive cocrystal, the side chains of Lys123 and Lys116, the MoaD C-terminal carboxylate of Gly77, and the C-1′ oxygen of precursor Z are all approximately 4 Å from each other (Figure 5C). In active MPT synthase, the presence of the bulkier thiocarboxylate at Gly77 would necessitate conformational changes in the active site. The most plausible scenario would be a shift of the MoaD C-terminus to the C-2′ position where there is less steric crowding. As seen in Figure 6A, superposition of

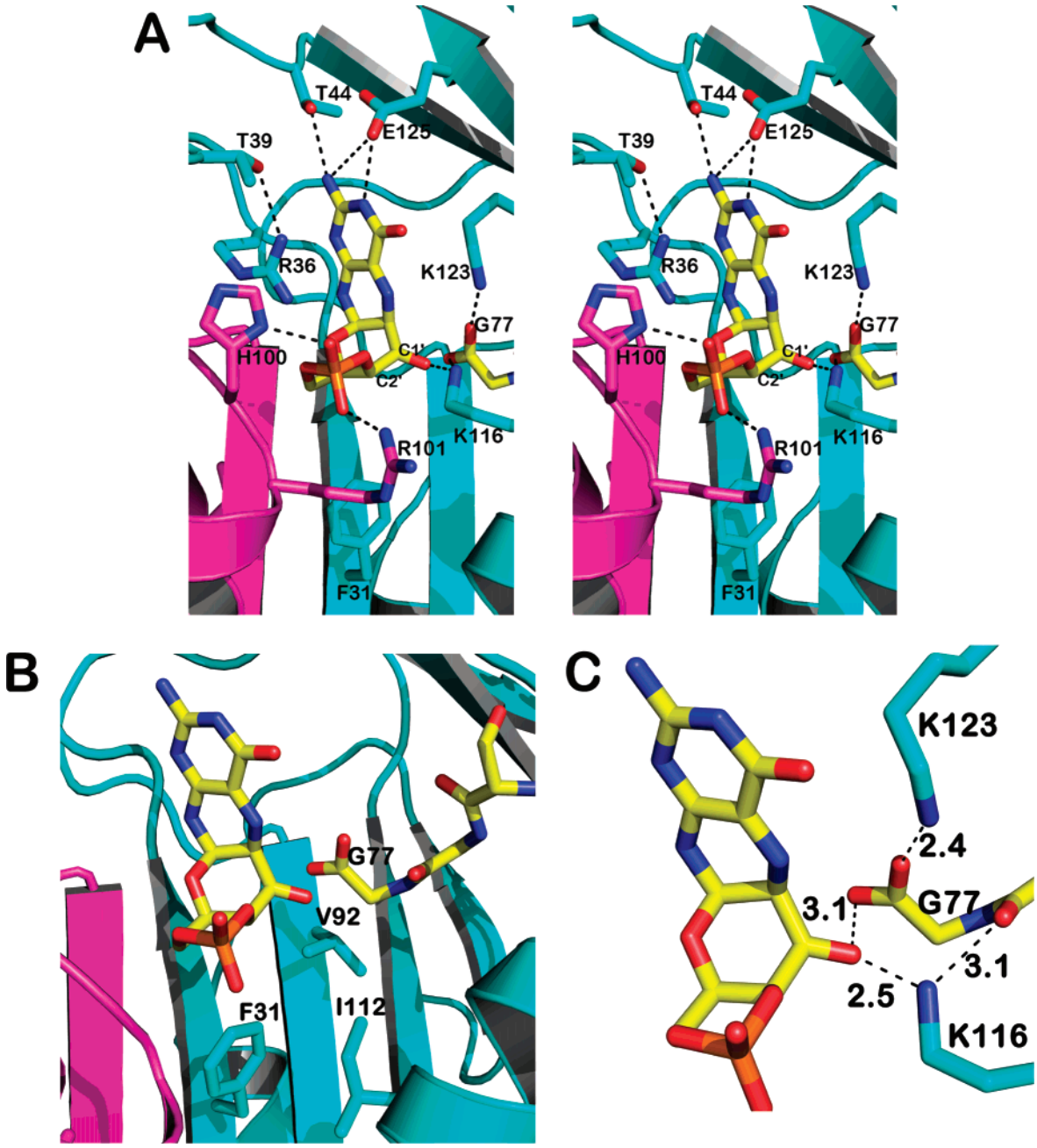

FIGURE 5: Substrate binding in the active site. (A) Close-up stereoview of the precursor Z binding pocket. Polar residues interacting with the substrate are shown with their side chains and the hydrogen bonds between the enzyme and its substrate as dashed lines. (B) Hydrophobic patch adjacent to the active site showing the strictly conserved Phe31 and type-conserved Val92 and Ile112. (C) Enlarged view of the C-terminal glycine of MoaD together with its surrounding residues with the distances between the polar atoms.

the MoaD C-terminal residues from the structure of activated (thiocarboxylated) *E. coli* MPT synthase PDB entry 3BII (*14*) onto the *S. aureus* MPT synthase−precursor Z complex reveals that in activated *S. aureus* MPT synthase, the MoaD C-terminal glycine would adopt a favorable conformation for attack at the C-2′ position of precursor Z. As described below, additional biochemical evidence for the addition of the first dithiolene sulfur to the C-2′ position was obtained through further structural characterization of the monosulfurated intermediate previously identified in *E. coli* MPT synthase reactions with the K126A MoaE variant (*30*).

Due to the extreme lability of Moco when it is released from molybdoenzymes, its structure was originally determined indirectly through the characterization of stable, oxidized derivatives of MPT. One of these derivatives, Form B, is generated when MPT is aerobically acidified to pH 2−3 and heated (*41*, *42*). As seen in Figure 1, this derivative retains the MPT C-2′ dithiolene sulfur atom in the form of a thiophene ring. Form B is structurally identical to the Moco catabolic end product, urothione (*41*, *42*), except for the methyl sulfide at the C-1′ position. To determine the side chain location of the single intermediate sulfur, an expression vector for the *S. aureus* K123A MoaE variant was created and the protein purified. MPT synthase reaction mixtures containing either *E. coli* K126A MoaE or *S. aureus* K123A MoaE along with precursor Z and their respective MoaD-SH partners were acidified to pH 2, boiled, and then analyzed by reversed phase HPLC for the presence of the fluorescent product Form B. Figure 6B (panel I) shows the elution position of control, dephosphorylated Form B generated from

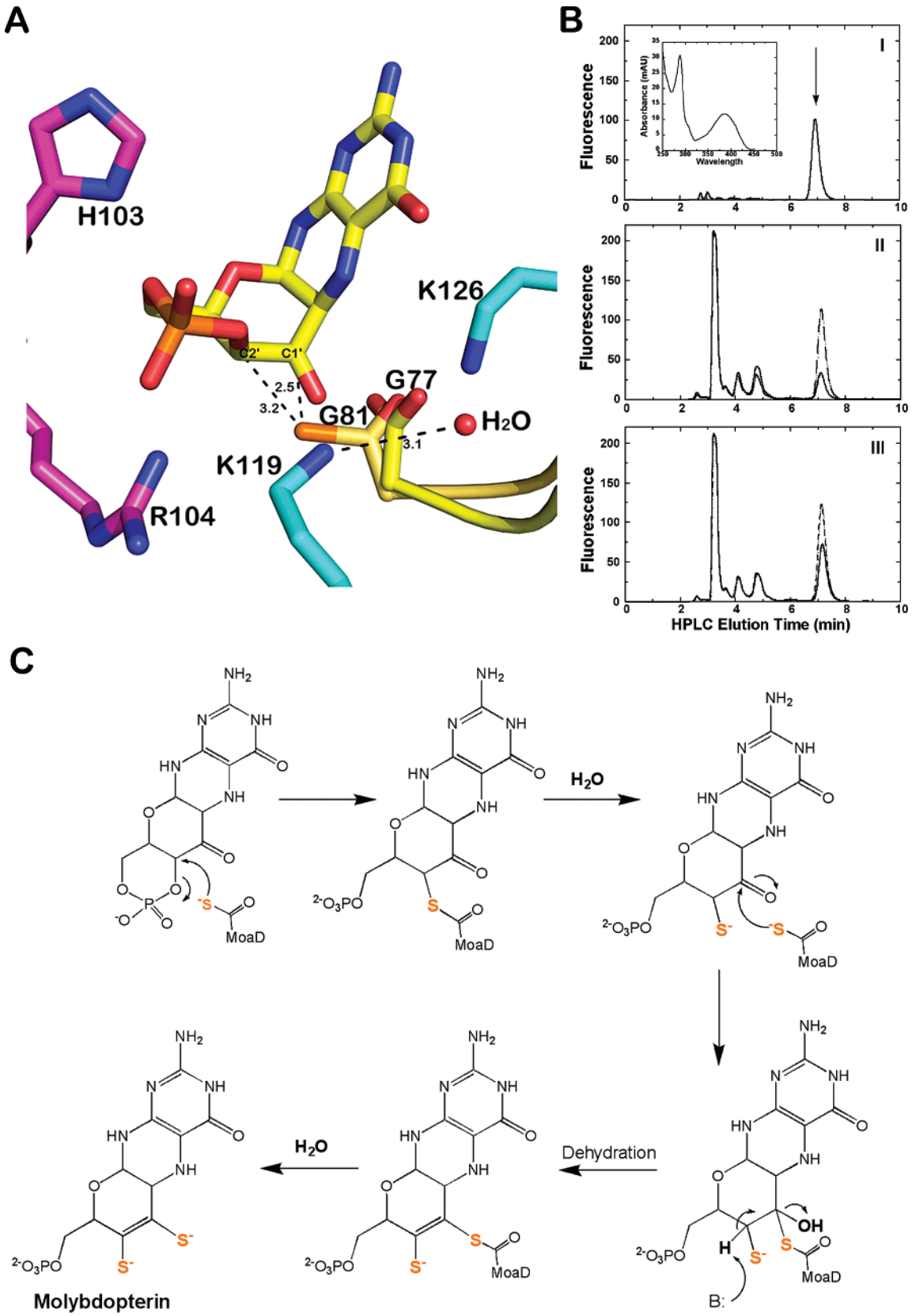

FIGURE 6: MPT synthase mechanism. (A) Superposition of *S. aureus* MoaD and precursor Z onto residues of activated *E. coli* MPT synthase (PDB entry 3BII). Proximal MoaE (cyan), distal MoaE (magenta), and the C-terminus of MoaD (tan, sulfur colored green). When the positions of the terminal glycines are compared, the thiocarboxylated terminus adopts a favorable conformation for attack at both the C-1′ and C-2′ positions. (B) Generation of Form B from the MPT synthase reaction intermediate. (Panel I) HPLC analysis of a 16 μL aliquot of the Form B control reaction. The arrow indicates the elution position of Form B, and the inset shows the online-spectrum of Form B. (Panel II) Overlay of the HPLC chromatograms obtained from 200 μL injections of the *S. aureus* K123A reaction (—) or the *E. coli* K126A reaction (- - -). (Panel III) Overlay of the co-injection of 100 μL aliquots of the K123A and K126A reactions (solid trace) or 8 μL of the Form B control reaction with 100 μL each of the K123A and K126A reactions. (C) Schematic diagram of the MPT synthase reaction mechanism.

the Moco-containing protein sulfite oxidase. As seen in panel II, when the HPLC chromatograms of the two MPT synthase reactions are overlaid, a fluorescent peak eluting at a position similar to the Form B control was observed in both reactions, suggesting that the *S. aureus* K123A MPT synthase reaction produces the same intermediate as the *E. coli* K126A reaction and that Form B can be generated from that intermediate. Coelution of the fluorescence peaks in panel II with each other (solid trace in panel III) as well as with the Form B control (dashed trace of panel III) supports these conclusions. Since the thiophene sulfur atom at the C-2′ position of Form B cannot be derived from a C-1′ sulfur, the generation of Form B from the intermediate indicates that its sulfur is located at C-2′ as shown in Figure 1. Therefore, the initial sulfur transfer during Moco biosynthesis occurs at this position.

Using this knowledge as well as evidence that MPT synthase is able to catalyze an identical reaction at two adjacent carbon atoms while the substrate remains bound at the same active site (*30*), the mechanistic proposal outlined in Figure 6C was formulated for MPT synthase. In this scheme, initial attack and transfer of the first MoaD-SH sulfur atom occur at the C-2′ position, and the transfer is coupled to hydrolysis of the precursor Z cyclic phosphate. This involves a direct attack of the thiocarboxylate sulfur on C-2′ resulting in an intermediate in which the MoaD C-terminus is covalently linked to the substrate via a thioester linkage. This adduct is subsequently hydrolyzed by a water molecule, and it is likely that the essential *E. coli* MoaE Lys119 residue (*S. aureus* Lys116) participates in this reaction. Consistent with this idea, there is a bound water molecule 3.1 Å from the amino group of Lys119 and 3.5 Å from the carbonyl carbon of the terminal glycine in the activated *E. coli* MPT synthase structure (Figure 6A) (*14*). The opening of the cyclic phosphate would shift the location of the intermediate to bind in a slightly different conformation in which the C-1′ atom has been pushed toward *E. coli* MoaE Lys126 or *S. aureus* Lys123 while the linearized phosphate remains ligated by the strictly conserved His-Arg pair from the distal MoaE subunit.

In the second step, a new MoaD thiocarboxylate would attack C-1′, resulting again in a covalent intermediate which is converted to molybdopterin via the elimination of a water molecule and hydrolysis of the thioester intermediate. The inability of the *E. coli* MoaE mutant corresponding to *S. aureus* K123A to further convert the monosulfurated intermediate to MPT suggests that this residue is involved in the sulfur transfer at the C-2′ position. Alternatively, it is possible that in this variant a structural change in the active site resulting from the smaller Ala side chain leads to nonproductive binding of the intermediate. Overall, this mechanism is similar to the sulfur transfer reaction mechanism observed during thiamine biosynthesis (*46*).

MPT Synthase Mutants Leading to Moco Deficiency. Almost all of the mutations that cause Moco deficiency belong to either of two groups, group A or group B, depending on whether the first or second step of Moco biosynthesis is affected. The members of the less common of the two groups, group B, generally exhibit mutations in *MOCS2A/B*, the genes encoding the human MPT synthase subunits. One group B mutation corresponds to the *E. coli* MoaE E128K mutation (*S. aureus* E125K) (*28*, *29*), and

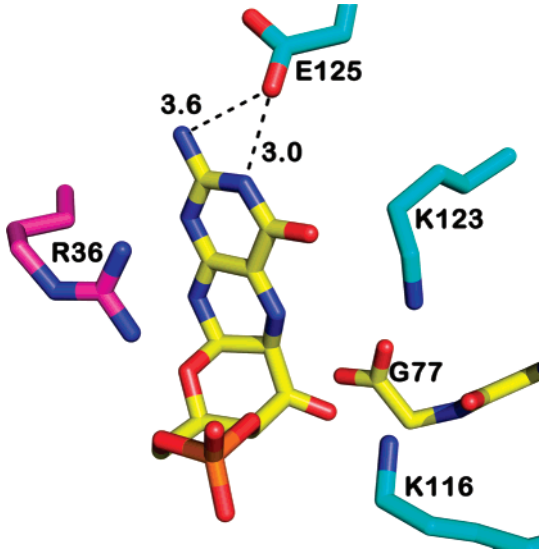

FIGURE 7: Structural basis of Moco deficiency. Close-up view of the interactions between Glu125 of MoaE and the N-1 and N-2 atoms of precursor Z in the *S. aureus* cocrystals.

biochemical studies of the *E. coli* variant indicated that this substitution decreased the activity of MPT synthase by a factor of 17 (*30*). Figure 7 shows a close-up view of the interaction between Glu125 and precursor Z in the *S. aureus* cocrystals. Modeling of the substitution of Glu125 with a lysine in this structure predicts close unfavorable contacts between precursor Z and the lysine side chain, resulting in the loss of the hydrogen bonds between the glutamate side chain and the precursor Z N-1 and N-2 atoms which would be expected to weaken or inhibit the binding of precursor Z.

Premature terminations after residues corresponding to Tyr5 of MoaD and Lys139 of MoaE were also observed in group B patients (*28*, *29*). The MoaD C-terminus is very sensitive to deletions and mutations (*47*) since it is the primary source of the ene-dithiolate S atoms, and the MoaD truncation is so severe that complete inactivation is certain. In the case of the MOCS2B truncation, the observed effect is surprising since the residues corresponding to this truncation are disordered in both the apo and precursor Z complex forms of *S. aureus* MPT synthase. Thus, it appears that these residues are not needed for a general stabilization of the enzyme or substrate binding. They could, however, be required to stabilize the monosulfurated intermediate in the active site by preventing its dissociation from the MoaE subunit, especially during the time period from the dissociation of the first MoaD subunit following the initial S transfer until a new thiocarboxylated MoaD subunit binds to deliver the second S atom.

The cocrystal structure of MPT synthase with precursor Z not only confirms the general location of the active site but also defines the substrate-binding and catalytically important residues in significantly more detail. In conjunction with biochemical experiments demonstrating that the first S atom is incorporated at the C-2′ position, this facilitates a significantly more detailed description of the MPT synthase catalytic mechanism. The structure also provides a rationale for understanding the effects of mutations in human MPT synthase leading to Moco deficiency.

ACKNOWLEDGMENT

We thank Liqun Wang (Stony Brook University) for technical assistance, Dr. Peter J. Tonge (Stony Brook University) for discussions about the enzyme mechanism, and Dr. Robert Haltiwanger (Stony Brook University) for critical reading of the manuscript.

NOTE ADDED AFTER PRINT PUBLICATION

Some of the data in Table 1 have been changed compared to the version published on the Web (ASAP) 12/20/07 and in the January 15, 2008, issue (Vol. 47, No. 2, pp 615−626). The correct electronic version of the paper was published 02/08/08, and an Addition and Correction appears in the March 11, 2008, issue (Vol. 47, No. 10).

REFERENCES

1. Rajagopalan, K. (1996) *Escherichia coli and Salmonella typhimurium*, Vol. 1, American Society for Microbiology, Washington, DC.
2. Hille, R. (1996) The Mononuclear Molybdenum Enzymes, *Chem. Rev. 96*, 2757−2816.
3. Johnson, J. L., and Wadman, S. K. (1989) *The metabolic basis of inherited disease*, McGraw-Hill, New York.
4. Johnson, J. L., Rajagopalan, K. V., Mukund, S., and Adams, M. W. (1993) Identification of molybdopterin as the organic component of the tungsten cofactor in four enzymes from hyperthermophilic Archaea, *J. Biol. Chem. 268*, 4848−4852.
5. Koshiba, T., Saito, E., Ono, N., Yamamoto, N., and Sato, M. (1996) Purification and properties of flavin- and molybdenum-containing aldehyde oxidase from coleoptiles of maize, *Plant Physiol. 110*, 781−789.
6. Lin, J. T., and Stewart, V. (1998) Nitrate assimilation by bacteria, *Adv. Microb. Physiol. 39*, 1−30, 379.
7. Campbell, W. H. (1996) Nitrate reductase biochemistry comes of age, *Plant Physiol. 111*, 355−361.
8. Menendez, C., Siebert, D., and Brandsch, R. (1996) MoaA of *Arthrobacter nicotinovorans* pAO1 involved in Mo-pterin cofactor synthesis is an Fe-S protein, *FEBS Lett. 391*, 101−103.
9. Hanzelmann, P., and Schindelin, H. (2004) Crystal structure of the S-adenosylmethionine-dependent enzyme MoaA and its implications for molybdenum cofactor deficiency in humans, *Proc. Natl. Acad. Sci. U.S.A. 101*, 12870−12875.
10. Wuebbens, M. M., Liu, M. T., Rajagopalan, K., and Schindelin, H. (2000) Insights into molybdenum cofactor deficiency provided by the crystal structure of the molybdenum cofactor biosynthesis protein MoaC, *Struct. Folding Des. 8*, 709−718.
11. Rudolph, M. J., Wuebbens, M. M., Rajagopalan, K. V., and Schindelin, H. (2001) Crystal structure of molybdopterin synthase and its evolutionary relationship to ubiquitin activation, *Nat. Struct. Biol. 8*, 42−46.
12. Pitterle, D. M., Johnson, J. L., and Rajagopalan, K. V. (1993) In vitro synthesis of molybdopterin from precursor Z using purified converting factor. Role of protein-bound sulfur in formation of the dithiolene, *J. Biol. Chem. 268*, 13506−13509.
13. Pitterle, D. M., and Rajagopalan, K. V. (1993) The biosynthesis of molybdopterin in *Escherichia coli*. Purification and characterization of the converting factor, *J. Biol. Chem. 268*, 13499−13505.
14. Rudolph, M. J., Wuebbens, M. M., Turque, O., Rajagopalan, K. V., and Schindelin, H. (2003) Structural studies of molybdopterin synthase provide insights into its catalytic mechanism, *J. Biol. Chem. 278*, 14514−14522.
15. Lake, M. W., Wuebbens, M. M., Rajagopalan, K. V., and Schindelin, H. (2001) Mechanism of ubiquitin activation revealed by the structure of a bacterial MoeB-MoaD complex, *Nature 414*, 325−329.
16. Leimkuhler, S., Wuebbens, M. M., and Rajagopalan, K. V. (2001) Characterization of *Escherichia coli* MoeB and its involvement in the activation of molybdopterin synthase for the biosynthesis of the molybdenum cofactor, *J. Biol. Chem. 276*, 34695−34701.
17. Xiang, S., Nichols, J., Rajagopalan, K. V., and Schindelin, H. (2001) The crystal structure of *Escherichia coli* MoeA and its relationship to the multifunctional protein gephyrin, *Structure 9*, 299−310.
18. Sandu, C., and Brandsch, R. (2002) Evidence for MoeA-dependent formation of the molybdenum cofactor from molybdate and molybdopterin in *Escherichia coli*, *Arch. Microbiol. 178*, 465−470.
19. Liu, M. T., Wuebbens, M. M., Rajagopalan, K. V., and Schindelin, H. (2000) Crystal structure of the gephyrin-related molybdenum cofactor biosynthesis protein MogA from *Escherichia coli*, *J. Biol. Chem. 275*, 1814−1822.
20. Schwarz, G., Schrader, N., Mendel, R. R., Hecht, H. J., and Schindelin, H. (2001) Crystal structures of human gephyrin and plant Cnx1 G domains: Comparative analysis and functional implications, *J. Mol. Biol. 312*, 405−418.
21. Llamas, A., Otte, T., Multhaup, G., Mendel, R. R., and Schwarz, G. (2006) The mechanism of nucleotide-assisted molybdenum insertion into molybdopterin. A novel route toward metal cofactor assembly, *J. Biol. Chem. 281*, 18343−18350.
22. Johnson, J. L., Indermaur, L. W., and Rajagopalan, K. V. (1991) Molybdenum cofactor biosynthesis in *Escherichia coli*. Requirement of the chlB gene product for the formation of molybdopterin guanine dinucleotide, *J. Biol. Chem. 266*, 12140−12145.
23. Johnson, J. L., Bastian, N. R., and Rajagopalan, K. V. (1990) Molybdopterin guanine dinucleotide: A modified form of molybdopterin identified in the molybdenum cofactor of dimethyl sulfoxide reductase from *Rhodobacter sphaeroides forma specialis denitrificans*, *Proc. Natl. Acad. Sci. U.S.A. 87*, 3190−3194.
24. Vergnes, A., Pommier, J., Toci, R., Blasco, F., Giordano, G., and Magalon, A. (2006) NarJ chaperone binds on two distinct sites of the aponitrate reductase of *Escherichia coli* to coordinate molybdenum cofactor insertion and assembly, *J. Biol. Chem. 281*, 2170−2176.
25. Neumann, M., Stocklein, W., and Leimkuhler, S. (2007) Transfer of the molybdenum cofactor synthesized by *Rhodobacter capsulatus* MoeA to XdhC and MobA, *J. Biol. Chem. 282*, 28493−28500.
26. Reiss, J. (2000) Genetics of molybdenum cofactor deficiency, *Hum. Genet. 106*, 157−163.
27. Reiss, J., and Johnson, J. L. (2003) Mutations in the molybdenum cofactor biosynthetic genes MOCS1, MOCS2, and GEPH, *Hum. Mutat. 21*, 569−576.
28. Reiss, J., Dorche, C., Stallmeyer, B., Mendel, R. R., Cohen, N., and Zabot, M. T. (1999) Human molybdopterin synthase gene: Genomic structure and mutations in molybdenum cofactor deficiency type B, *Am. J. Hum. Genet. 64*, 706−711.
29. Leimkuhler, S., Charcosset, M., Latour, P., Dorche, C., Kleppe, S., Scaglia, F., Szymczak, I., Schupp, P., Hahnewald, R., and Reiss, J. (2005) Ten novel mutations in the molybdenum cofactor genes MOCS1 and MOCS2 and in vitro characterization of a MOCS2 mutation that abolishes the binding ability of molybdopterin synthase, *Hum. Genet. 117*, 565−570.
30. Wuebbens, M. M., and Rajagopalan, K. V. (2003) Mechanistic and mutational studies of *Escherichia coli* molybdopterin synthase clarify the final step of molybdopterin biosynthesis, *J. Biol. Chem. 278*, 14523−14532.
31. Wuebbens, M. M., and Rajagopalan, K. V. (1993) Structural characterization of a molybdopterin precursor, *J. Biol. Chem. 268*, 13493−13498.
32. Otwinowski, A., and Minor, W. (1997) *Methods in Enzymology*, Macromolecular Crystallography, Vol. 276A, Academic Press, San Diego.
33. Vagin, A. A., and Isupov, M. N. (2001) Spherically averaged phased translation function and its application to the search for molecules and fragments in electron-density maps, *Acta Crystallogr. D57*, 1451−1456.
34. Vagin, A., and Teplyakov, A. (2000) An approach to multi-copy search in molecular replacement, *Acta Crystallogr. D56*, 1622−1624.
35. Murshudov, G. N., Vagin, A. A., and Dodson, E. J. (1997) Refinement of macromolecular structures by the maximum-likelihood method, *Acta Crystallogr. D53*, 240−255.
36. Winn, M. D., Isupov, M. N., and Murshudov, G. N. (2001) Use of TLS parameters to model anisotropic displacements in macromolecular refinement, *Acta Crystallogr. D57*, 122−133.
37. Winn, M. D., Murshudov, G. N., and Papiz, M. Z. (2003) Macromolecular TLS refinement in REFMAC at moderate resolutions, *Methods Enzymol. 374*, 300−321.
38. Jones, T. A., Zou, J. Y., Cowan, S. W., and Kjeldgaard, M. (1991) Improved methods for building protein models in electron density

maps and the location of errors in these models, *Acta Crystallogr. A47* (Part 2), 110−119.
39. Bailey, S. (1994) The CCP4 suite: Programs for protein crystallography, *Acta Crystallogr. D50*, 760−763.
40. Perrakis, A., Morris, R., and Lamzin, V. S. (1999) Automated protein model building combined with iterative structure refinement, *Nat. Struct. Biol. 6*, 458−463.
41. Johnson, J. L., and Rajagopalan, K. V. (1982) Structural and metabolic relationship between the molybdenum cofactor and urothione, *Proc. Natl. Acad. Sci. U.S.A. 79*, 6856−6860.
42. Johnson, J. L., Hainline, B. E., Rajagopalan, K. V., and Arison, B. H. (1984) The pterin component of the molybdenum cofactor. Structural characterization of two fluorescent derivatives, *J. Biol. Chem. 259*, 5414−5422.
43. Lovell, S. C., Davis, I. W., Arendall, W. B., III, de Bakker, P. I., Word, J. M., Prisant, M. G., Richardson, J. S., and Richardson, D. C. (2003) Structure validation by Cα geometry: ϕ,ψ and Cβ deviation, *Proteins 50*, 437−450.
44. Johnson, J. L., Wuebbens, M. M., and Rajagopalan, K. V. (1989) The structure of a molybdopterin precursor. Characterization of a stable, oxidized derivative, *J. Biol. Chem. 264*, 13440−13447.
45. Santamaria-Araujo, J. A., Fischer, B., Otte, T., Nimtz, M., Mendel, R. R., Wray, V., and Schwarz, G. (2004) The tetrahydropyranopterin structure of the sulfur-free and metal-free molybdenum cofactor precursor, *J. Biol. Chem. 279*, 15994−15999.
46. Vander Horn, P. B., Backstrom, A. D., Stewart, V., and Begley, T. P. (1993) Structural genes for thiamine biosynthetic enzymes (*thiCEFGH*) in *Escherichia coli* K-12, *J. Bacteriol. 175*, 982−992.
47. Schmitz, J., Wuebbens, M. M., Rajagopalan, K. V., and Leimkuhler, S. (2007) Role of the C-terminal Gly-Gly motif of *Escherichia coli* MoaD, a molybdenum cofactor biosynthesis protein with a ubiquitin fold, *Biochemistry 46*, 909−916.

BI701734G